JGR Oceans

RESEARCH ARTICLE
10.1029/2023JC019865

Key Points:

- Chlorophyll-a concentration has increased over the last 24 years in most of the Southwestern Atlantic
- Phytoplankton phenological changes have been observed, mainly during the austral autumn bloom
- Phytoplankton biomass and phenology might be affected by the increasing sea surface temperature and mixing layer depth shoaling

Supporting Information:

Supporting Information may be found in the online version of this article.

Correspondence to:

A. L. Delgado and G. Basterretxea,
aldelgado@iado-conicet.gob.ar;
gotzon@imedea.uib-csic.es

Citation:

Delgado, A. L., Hernández-Carrasco, I., Combes, V., Font-Muñoz, J., Pratolongo, P. D., & Basterretxea, G. (2023). Patterns and trends in Chlorophyll-a concentration and phytoplankton phenology in the biogeographical regions of Southwestern Atlantic. *Journal of Geophysical Research: Oceans*, *128*, e2023JC019865. https://doi.org/10.1029/2023JC019865

Received 24 MAR 2023
Accepted 10 AUG 2023

Author Contributions:

Conceptualization: Ana L. Delgado, Gotzon Basterretxea
Formal analysis: Ana L. Delgado, Ismael Hernández-Carrasco, Vincent Combes, Joan Font-Muñoz, Paula D. Pratolongo, Gotzon Basterretxea
Funding acquisition: Ana L. Delgado, Gotzon Basterretxea
Investigation: Ana L. Delgado
Methodology: Ana L. Delgado, Ismael Hernández-Carrasco, Vincent Combes, Joan Font-Muñoz, Gotzon Basterretxea

Patterns and Trends in Chlorophyll-a Concentration and Phytoplankton Phenology in the Biogeographical Regions of Southwestern Atlantic

Ana L. Delgado[1,2], Ismael Hernández-Carrasco[3], Vincent Combes[3,4], Joan Font-Muñoz[3], Paula D. Pratolongo[5,6], and Gotzon Basterretxea[3]

[1]Instituto Argentino de Oceanografía (IADO-CONICET-UNS), Bahía Blanca, Argentina, [2]Departamento de Geografía y Turismo, Universidad Nacional del Sur (UNS), Bahía Blanca, Argentina, [3]Institut Mediterrani d'Estudis Avançats (IMEDEA-CSIC-UIB), Esporles, Spain, [4]Departament de Física, Universitat de les Illes Balears, Palma de Mallorca, Spain, [5]Centro de Recursos Renovables de la Región Semiárida (CERZOS-CONICET-UNS), Bahía Blanca, Argentina, [6]Departamento de Biología, Bioquímica y Farmacia, Universidad Nacional del Sur (UNS), Bahía Blanca, Argentina

Abstract The Southwestern Atlantic Ocean (SWA), is considered one of the most productive areas of the world, with a high abundance of ecologically and economically important fish species. Yet, the biological responses of this complex region to climate variability are still uncertain. Here, using 24 years of satellite-derived Chl-a data, we classified the SWA into 9 spatially coherent regions based on the temporal variability of Chl-a concentration, as revealed by SOM (Self-Organizing Maps) analysis. These biogeographical regions were the basis of a regional trend analysis in phytoplankton biomass, phenological indices, and environmental forcing variations. A general positive trend in phytoplankton concentration was observed, especially in the highly productive areas of the northern shelf-break, where phytoplankton biomass has increased at a rate of up to 0.42 ± 0.04 mg m^{-3} per decade. Significant positive trends in sea surface temperature were observed in 4 of the 9 regions (0.08–0.26 °C $decade^{-1}$) and shoaling of the mixing layer depth in 5 of the 9 regions (−1.50 to −3.36 m $decade^{-1}$). In addition to the generally positive trend in Chl-a, the most conspicuous change in the phytoplankton temporal patterns in the SWA is a delay in the autumn bloom (between 15 ± 3 and 24 ± 6 days $decade^{-1}$, depending on the region). The observed variations in phytoplankton phenology could be attributed to climate-induced ocean warming and extended stratification period. Our results provided further evidence of the impact of climate change on these highly productive waters.

Plain Language Summary The Southwestern Atlantic Ocean (SWA), is one of the most biologically productive areas of the world, with a high abundance of fish species. This important area might be affected by the environmental consequences of climate change. In this study, we addressed the influence of the already observed changes in environmental conditions on phytoplankton, which are the base of the marine food web, over the last 24 years. There has been an increase in phytoplankton biomass as well as the timing and intensity of the autumn bloom in some specific areas of the SWA. We have found that these changes in phenology might be related to the increase in sea surface temperature and the shoaling of the mixed layer depth. Consistent with previous studies, our results provided further evidence of the impact of climate change on these highly productive waters.

1. Introduction

Phytoplankton are at the base of the ocean foodwebs and plays a major role in CO_2 fluxes. Indeed, it roughly produces 50 Gt of organic C yr^{-1}, corresponding to ∼40% of annual global primary productivity, contributing to the uptake of more than 23% of total anthropogenic CO_2 emissions into the atmosphere (Friedlingstein et al., 2019). Phytoplankton species composition, seasonal bloom initiation, duration, and intensity, as well as the overall productivity of the ocean, are predicted to change in response to variations in water temperature, nutrients supply, and acidification derived from ongoing climate change (Doney et al., 2012). Since phytoplankton growth is mostly controlled by light and nutrient availability, it is tightly linked to the dynamics of the ocean surface mixed layer (Longhurst, 2007). Atmospheric forcing and large-scale climate variability patterns, together with top-down controls (i.e., grazing), modulate phytoplankton phenological cycles (Zhai et al., 2013). These variations in the canonical patterns influence productivity at higher trophic levels. However, anticipating these ecosystem-level changes in the future ocean remains challenging since phytoplankton include phylogenetically

Project Administration: Ana L. Delgado, Gotzon Basterretxea
Writing – original draft: Ana L. Delgado
Writing – review & editing: Ana L. Delgado, Ismael Hernández-Carrasco, Vincent Combes, Joan Font-Muñoz, Paula D. Pratolongo, Gotzon Basterretxea

diverse organisms with different metabolic responses and evolutionary backgrounds (Anderson et al., 2021; Dutkiewicz et al., 2013).

The Southwestern Atlantic Ocean (SWA) is recognized as a vast sink for atmospheric and anthropogenic CO_2 via biological and solubility pump processes (Sigman et al., 2010). Indeed, it is regarded as one of the most important regions for the global carbon cycle (Field et al., 1998). Within the SWA, from the tip of South America (~55°S) to the Brazil/Malvinas Confluence (~38°S) lies the Patagonian shelf, one of the most biologically productive and largest carbon sinks in the world (Figure 1, García et al., 2008; Lutz et al., 2010). This region is characterized by intense and complex ocean dynamics (i.e., coastal upwelling, thermo-haline circulation, tidal forcing; Acha et al., 2004) that favor high ocean productivity, including extensive phytoplankton blooms (e.g., Alvain et al., 2008; Delgado et al., 2019; Guinder et al., 2018; Segura et al., 2021). Due to its hydrographic complexity, high biological productivity, freshwater inputs, and interoceanic connections, nutrients present high variability in the study area (nitrate: 0.2–32 μM; silicate: 0.1–60 μM; ammonium: 0.1–1.6 μM; phosphate: 0.4–1.9 μM) (Garzón-Cardona et al., 2019; Lara et al., 2010). As a result of climate change, the SWA displays evidence of profound changes which have been associated the with progressive sea warming of surface waters (Hobday & Pecl, 2014), changes in wind forcing (Leyba et al., 2019), poleward migration of western boundary currents (Artana et al., 2019) and intensification and/or increase in the frequency and intensity of climate-forced variability events (ENSO, Southern Annular Mode, droughts, heatwaves; e.g., Cai et al., 2020; Risaro et al., 2022).

The classification of marine areas into biogeographical regions sharing similar properties and dynamics has become essential to understand the responses of marine ecosystems in highly complex areas, such as the SWA, to environmental forces in present and future climate scenarios (Basterretxea et al., 2018). In addition, the classification of the marine environment into biogeographic regions contributes to the understanding of ecosystem functions, very useful to define local (or specific) indicators of ecosystem state, supporting the establishment of resource management and conservation policies (Spalding et al., 2007). Satellite ocean-color data provide synoptic and long-term coverage, which is ideal for regionalization studies. The neural network-based Self-Organizing Maps (SOM) technique has demonstrated high efficiency to cluster and identifying patterns in large datasets (Kohonen, 1982; Vesanto & Alhoniemi, 2000). SOM classification has been used for a variety of applications including the synthesis of spatial patterns of chlorophyll-a (Chl-a) and the classification of spectral signals for subsequent inference of phytoplankton groups (e.g., Basterretxea et al., 2018; Ben Mustapha et al., 2014; Saraceno et al., 2006; Yala et al., 2020). SOM can be applied to both space and time domains of the analyzed variable, providing, a powerful analysis tool for diagnosing ocean processes (Hernández-Carrasco & Orfila, 2018; Liu et al., 2016).

The present work aims at characterizing the spatial patterns and long-term trends of Chl-a concentration and phytoplankton phenology in the SWA, and their relation with ongoing climate-induced environmental changes in the region. Using 24 years of satellite-derived Chl-a datasets, we first classified the SWA into coherent regions based on homogeneous temporal variability of Chl-a concentration, as revealed by the SOM analysis. These coherent biogeographical regions were the basis of our regional trend analysis in phytoplankton biomass, phenological indices, and environmental forcing variations. The observed changes in phytoplankton biomass and phenology, as well as the related environmental changes, are key to understanding regional functional and structural aspects of marine communities in the SWA, allowing to set a potential strategy to detect and monitor crucial regions.

2. Materials and Methods

2.1. Data Sources

Our analysis is based on the sea surface Chl-a (mg m^{-3}) merged product provided by the GlobColour project (distributed by ACRI ST, France: https://hermes.acri.fr/). A spatial subset of the study area (Figure 1) was extracted from a time series of the 8-day L3 Chl-a product at 4 km resolution for the period 1998–2021 (24 years). This ocean color product is the result of merging SeaWiFS, MERIS, MODIS-Aqua, and OLCI sensors and estimates the average Chl-a concentration over the first optical depth (Maritorena et al., 2010). Merging data from different satellite sensors is an effective method for increasing the study period of ocean-color satellites to enable climate-scale studies (Maritorena & Siegel, 2005). The Chl-a algorithms used to develop this product were validated in the SWA with in-situ data acquired between 2001 and 2019 obtaining accurate results (Delgado et al., 2021, $R^2 = 0.84$, RMSE = 1.51; Dogliotti et al., 2009, $R^2 = 0.89$, RMSE-log = 0.29). Moreover,

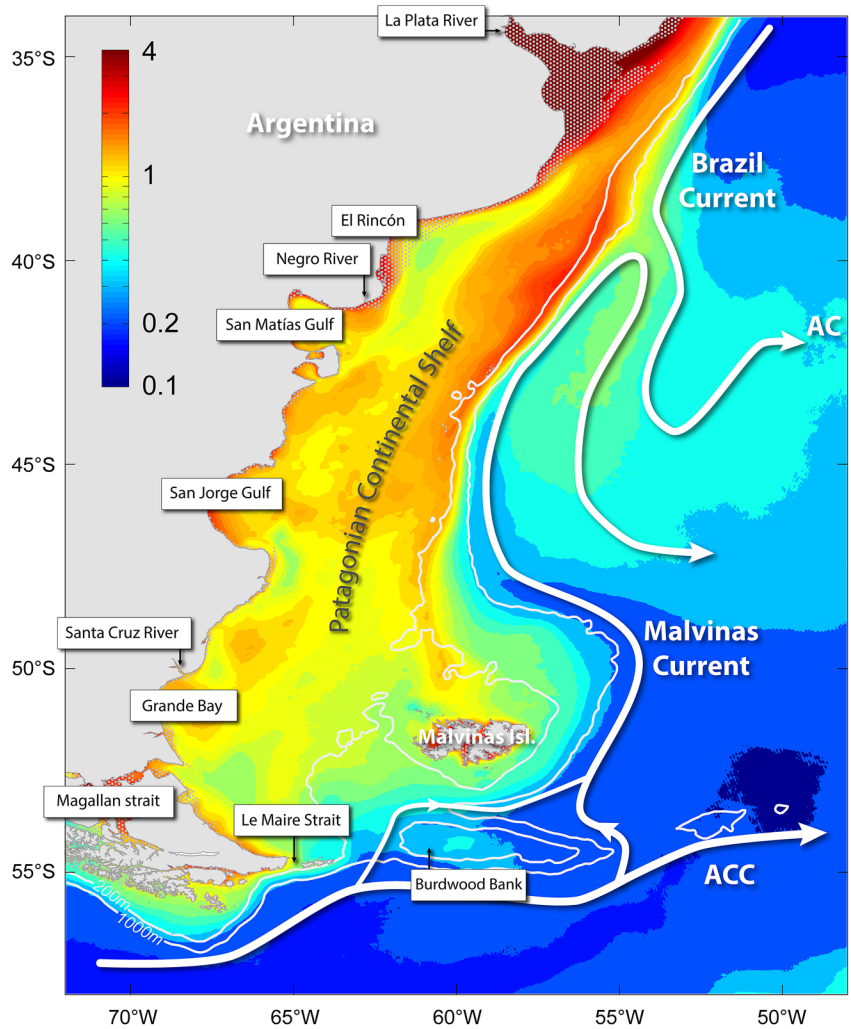

Figure 1. Mean Chlorophyll-a concentration (mg m^{-3}) in the Southwestern Atlantic Ocean (SWA) for the period (1998–2021) and, overlapped, main circulation patterns (thick arrows). Dotted areas (i.e., in La Plata River) indicate biased chlorophyll-a values that were excluded from the analysis.

the GlobColour merged product presents good accuracy when compared to in-situ Chl-a data (R^2 = 0.81, Bias = 0.03; Garnesson et al., 2019). Even though this product has not been climatology bias-corrected, as OC-CCI (Sathyendranath et al., 2019), both products present similar accuracy results (Yu et al., 2023). In addition, the flagging criteria used by GlobColour enable higher spatial and temporal coverage (Garnesson et al., 2019). Since global algorithms (based on blue-to-green ratios) do not perform well in the optically complex waters of the inner Argentinean continental shelf (Armstrong et al., 2004; Delgado et al., 2021; Williams et al., 2013), we masked the coastal waters located at depths <25 m to avoid biased results.

Physical variables used for the environmental characterization were obtained from the Global Ocean Physics Reanalysis provided by CMEMS (GLORYS12v1). GLORYS provides monthly SST, monthly Mixed Layer Depth (MLD), and Sea Surface Salinity (SSS), among other physical variables, at 1/12° spatial resolution. GLORYS is available from Copernicus Marine Environment Monitoring Service (CMEMS, https://data.marine.copernicus.eu) and is based on the current real-time global high-resolution forecasting CMEMS system PSY4V3 (Lellouche et al., 2018). The model outputs are reliable for trend analysis (SST, bias <0.01°C; SSS, bias <0.2; Drévillon et al., 2022).

2.2. Biogeographical Regionalization

Biogeographical regions within the study area were defined based on the analysis of satellite-derived Chl-a using SOM. SOM is a type of artificial neural network that is trained using an unsupervised learning algorithm. This

technique is especially suited for feature extraction and pattern recognition in large data sets (Kohonen, 1982, 1990). SOM is a nonlinear mapping method that projects high-dimensional data onto a low-dimensional space, preserving the topology of the original data set. As a result, SOM can summarize the information contained in large time series of georeferenced variables, into a single map of a few patterns (Liu et al., 2016). When SOM is applied to the time domain of Chl-a satellite data, distinctive temporal patterns of Chl-a concentration can be inferred, allowing the identification of regions having a similar phytoplankton dynamic (Basterretxea et al., 2018).

We selected a network of 3 × 3 neurons or units. Increasing the number of neurons, for instance using a neural network of size of 4 × 4 and 4 × 3, more detailed temporal patterns and more regions of Chl-a variability emerge. However, these new patterns only split the boundaries of regions inferred from the 3 × 3 SOM, without providing relevant insight into regions with different biochemical or physical behavior. Furthermore, using a larger number of neurons can result in fictitious patterns (with zero probability of occurrence), which are not representative of the analyzed data set (Basterretxea et al., 2018; Hernández-Carrasco & Orfila, 2018; Liu et al., 2006).

For the analysis, we used the SOM v.2.0 MATLAB toolbox (Vesanto et al., 2000) distributed by the Helsinki University of Technology (http://www.cis.hut.fi/somtoolbox/), adapted to handle long time series of satellite data. In our computations, we use a sheet and hexagonal map lattice configuration, guaranteeing that the distance between the neuron and all its associated neighbors is the same. Each neuron has assigned a weighted vector of Chl-a values randomly generated during the initialization. In the training process, the neural network is transformed through an iterative presentation of the previously normalized satellite Chl-a data. In each iteration (or epoch), the neuron whose weight vector is more similar (in terms of Euclidean distance) to the input data vector, termed the Best-Matching Unit, is updated together with its topological neighbors toward the input sample following a neighborhood function. Following Liu et al. (2006), we opted for a "Ep" type neighborhood function and a batch training algorithm, as this combination yields the most accurate patterns (i.e., lower quantitative and topological errors) and low computational cost. After repeating the training process iteratively (100 epochs in our case), until a stable convergence of the map is achieved, we obtain a neural network with the final time variability patterns of Chl-a concentration. The resulting patterns will exhibit some similarity because the SOM process assumes that a single sample of data (one input vector) contributes to the creation of more than one pattern, as the whole neighborhood around the best matching pattern is also updated in each step of training.

2.3. Phytoplankton Phenology

Phytoplankton phenology was analyzed using the characteristic Chl-a time series obtained for each biogeographical region from the SOM analysis. The obtained SOM time series was processed with TIMESAT software, which was developed to explore time series of vegetation indices with a regular cyclicity and to retrieve the phenology metrics (Jönsson & Eklundh, 2004; Palmer et al., 2015). TIMESAT has been successfully applied to study phytoplankton phenology in diverse aquatic environments (Benzouaï et al., 2020; Palmer et al., 2015; Shi et al., 2019). The characteristic time series was low-pass filtered with a Savitzky-Golay filter (window size 4) to reduce high-frequency variations. A common practice is to define the start of a seasonal bloom event when the Chl-a concentration rises above the background median plus 5%–20%, depending on the typical Chl-a concentrations of the region (Racault et al., 2012; Zoljoodi et al., 2022). In our case, Chl-a concentrations are relatively high (0.1–14 mg m^{-3}). Thus, to avoid the interference of short-term peaks, we chose a Chl-a concentration of 20% above the median as a threshold to identify the start of the seasonal bloom. Accordingly, the end of the bloom was established when the Chla-a concentration fell under the same threshold. Four essential indices proposed by Racault et al. (2012) were used to characterize phytoplankton phenology: the timing of the main bloom initiation (b_i), the peak intensity (p_k), the timing of the main bloom termination (b_e) and the bloom duration. The same indices were used when a secondary bloom was observed.

2.4. Trend Analysis

Census X-13 was used to produce a seasonally adjusted series, removing seasonality from the Chl-a time series of each SOM-defined biogeographical region. The Census X-13 is an improved version of Census X-11. Its application to time series analysis of satellite ocean color data has been extensively documented (Delgado et al., 2015; Salgado-Hernanz et al., 2019; Vantrepotte & Mélin, 2009). The method is based on the iterative bandpass-filtering procedure that allows for the definition of a non-periodical seasonal term, to specifically assess

the inter-annual variation in the time series seasonality (in terms of period and amplitude). The relative part of the variance of the components is estimated for each grid point, to identify the spatial patterns of the temporal variability in the series. This method aims at decomposing a time series $X(t)$ into three additive components:

$$X(t) = S(t) + T(t) + I(t)$$

where S is the seasonal signal, T is the trend cycle signal and I is the irregular or residual signal (Shiskin, 1978; Vantrepotte & Mélin, 2009).

Several successive steps are applied to decompose the series. First, an initial estimate of the trend-cycle component $T(t)$ is obtained from the annual-centered running average of the original series $X(t)$. A seasonal running mean is then applied to the trend-adjusted series ($X(t) - T(t)$) to derive seasonal coefficients that are uncontaminated with the inter-annual trend. The resulting series is then normalized by subtracting its annual-centered running average, leading to a seasonal series $S(t)$ with approximately a null mean value. An improved estimate of the trend component $T(t)$ is obtained by applying an annual filter to the seasonally adjusted series ($X(t) - S(t)$). In this case, a Henderson (1916) trend filter is applied instead of the simple annual-centered running average. This filter smooths the series while preserving the local polynomial trends of orders 2 and 3. Finally, to derive a refined estimate of the seasonal component, $S(t)$, a seasonal running mean is applied to the revised trend-adjusted series ($X(t) - T(t)$). To obtain the final estimate of the trend component $T(t)$, the Henderson trend filter is applied to the revised seasonally adjusted series ($X(t) - S(t)$). The residual series that accounts for sub-annual variations is calculated as $I(t) = X(t) - S(t) - T(t)$.

In addition, we tested for the presence of monotonic upward or downward trends in the time series of Chl-a, environmental variables, and phenological estimates, for each biogeographical region. We used the non-parametric seasonal Kendall test, based on the calculation of a set of Mann–Kendall statistics applied to each separatemonth, which are then combined to evaluate the existence of long-term monotonic changes in the original time series (Hirsch et al., 1982). We used Sen's slope, a non-parametric slope estimator from Sen (1968) and adapted by Hirsch et al. (1982) to estimate the magnitude of each time series' trend, expressed in mg m^{-3} $decade^{-1}$ (Chl-a, p_k), days $decade^{-1}$ (b_i, b_e, and b_d), m $decade^{-1}$ (MLD), or °C $decade^{-1}$ (SST) (Gilbert, 1987; Ibanez & Conversi, 2002; Vantrepotte & Mélin, 2011).

3. Results

3.1. Biogeographical Regionalization

The 9 biogeographical regions and their characteristic temporal patterns and climatologies obtained from the SOM analysis are shown in Figure 2. The patterns are topologically ordered according to the mean value and variance. For instance, patterns with large variability and higher mean values of Chl-a concentration are located at the top-right corner of the neural network, whereas those with low variability and low mean Chl-a concentrations are located around the bottom-left corner.

The less productive regions (R1, R2, and R3) jointly comprise 66% of the study area and mainly represent oceanic waters off the shelf. R3 is characterized by the lowest mean Chl-a concentration and variability of the whole study area (0.41 ± 0.18 mg m^{-3}) and includes the southern section of the study area where the Antarctic Circumpolar Current flows through the Drake Passage and the Burdwood Bank. R1 is the second largest region, extending over 22% of the study area. The mean Chl-a concentration in this region is twofold that in R1 (0.83 ± 0.36 mg m^{-3}). Most of the coastal Patagonian tidal fronts, from the southern portion of San Matías Gulf until Grande Bay (southern margin of Argentina) lie within R1, as well as the northern retroflection of Malvinas Current (MC; Figure 1). R2 corresponds to the northern inner shelf waters of the study area (El Rincón and Norpatagonian Gulfs) and to the oceanic waters located outside the shelf break north of 44°S (0.74 ± 0.29 mg m^{-3}), where the retroflection of Brazil Current is located (R1).

R4 and R5 represent transition regions between the open ocean waters and the highly productive regions over the southern shelf and shelf break. R4 is geographically located in the mid-shelf waters of the Northern Patagonian continental shelf. Compared with the previously described regions, the mean value of Chl-a concentration and its variability is higher (1.37 ± 0.7 mg m^{-3}). Region R5 is a highly productive region (1.52 ± 0.97 mg m^{-3}) that encompasses the San Jorge Gulf and La Isla Escondida area.

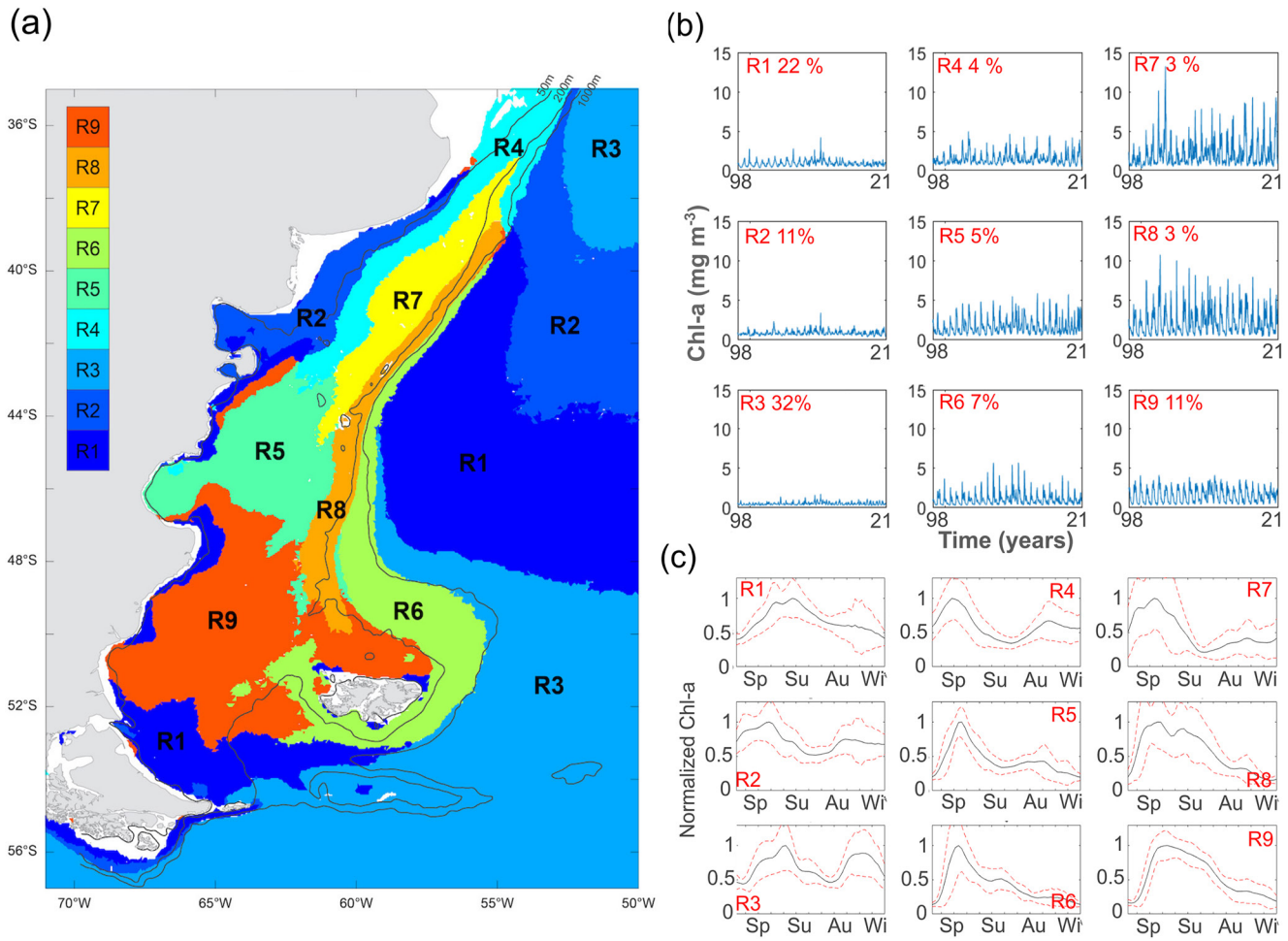

Figure 2. (a) Biogeographical classification of Chl-a depicted from the 3 × 3 Self-Organizing Map (SOM) classification. (b) Characteristic Chl-a temporal patterns obtained from SOM computation. The inset number in red indicates the percentage of pixels clustered in each neuron. (c) Normalized climatology of the Chl-a temporal patterns. The solid black line indicates the mean and dashed red lines indicate ± one standard deviation. Sp = Spring, Su = Summer, Au=Autumn, Wi = Winter.

Regions characterized by the patterns shown in the upper right corner of the neural network (R7, R8, and R6, Figures 2b and 2c) represent the main hot spots of primary production in the Southwestern Atlantic Ocean, with chlorophyll-a concentrations exceeding in some cases 10 mg m^{-3}. The SOM analysis identifies three distinct subzones in this frontal area. Region 7 represents the north-western section of the shelf-break front, between 37 and 44°S and located in the mid-shelf/outer-shelf, within the Argentinean Continental waters (2.08 ± 1.7 mg m^{-3}). R8 spans along the shelf-break, between ~38° and 49°S, with elevated mean Chl-a concentrations (2.13 ± 1.65 mg m^{-3}). Finally, R6 extends between the 200 and 1,000 m isobath, from 40°S to the north-western border of the Malvinas Islands. This region exhibits mean values of Chl-a comparable to R1, R2, and R3 but a higher variability (0.92 ± 0.75 mg m^{-3}).

Finally, R9 presents some similarities to R6, according to topological ordering of SOM. This region encompasses the Patagonian cold estuarine zone, off the coast of southern Patagonia, characterized by relatively high mean values and variability of Chl-a concentration (1.4 ± 0.9 mg m^{-3}). R9 extends from the outer region of the Peninsula Valdez front to the northern area of the Malvinas Islands, where it overlaps with the southern boundary of the SBF.

3.2. Phytoplankton Phenology

Phytoplankton phenology indices are displayed in Figure 3. All regions exhibit a main bloom in austral spring (September–December). Additionally, some regions show a secondary peak in austral autumn (March–June;

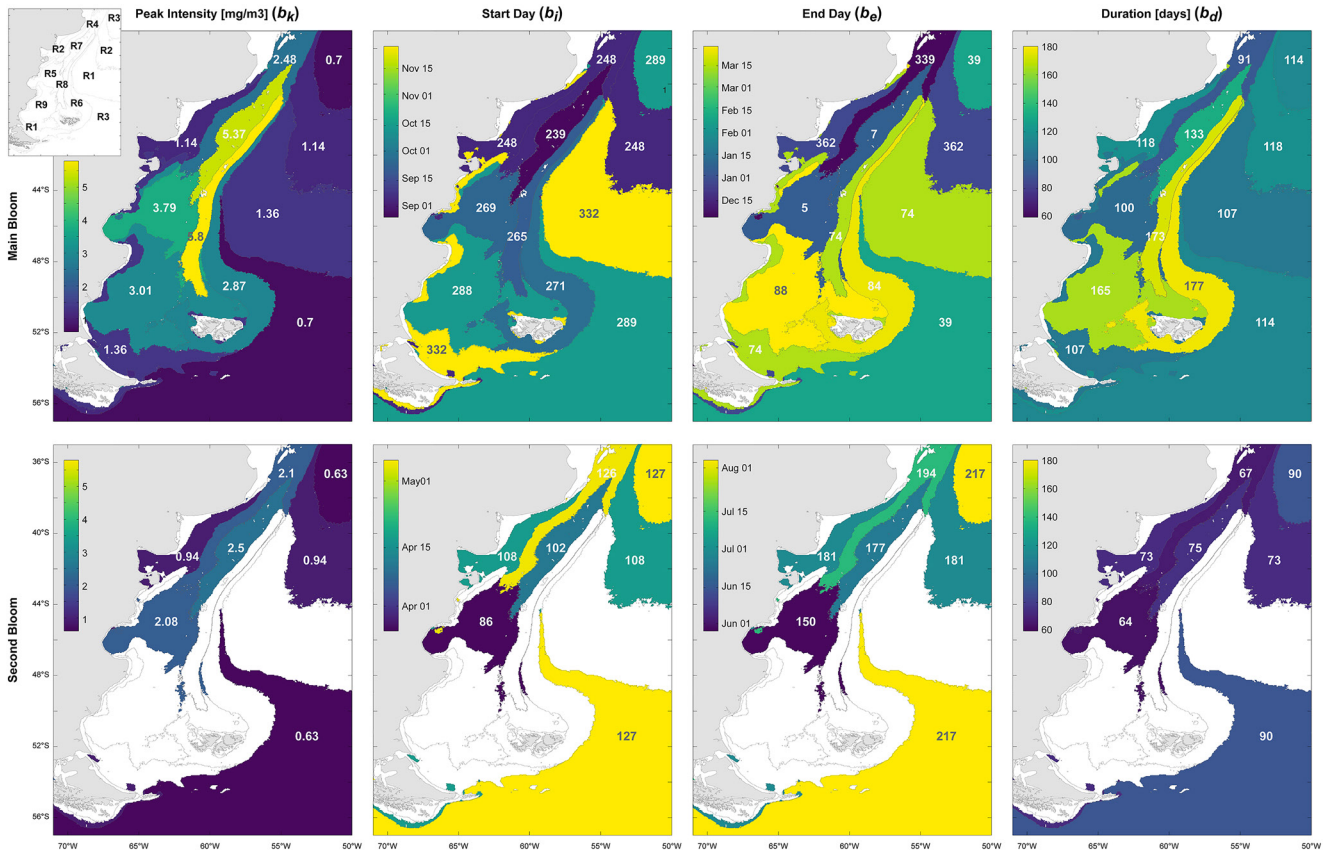

Figure 3. Climatology of the main (upper panel) and secondary (lower panel) bloom phenological indices. The b_i and b_e dates are expressed as Julian days. b_d is expressed in days and the b_k in mg Chl-a m^{-3} (Standard deviation and significance values are shown in Table S1 in Supporting Information S1).

Figure 3). It is worth mentioning that bloom detection was based on threshold values and, in some regions, there were calendar years in which blooms were not detected. This was more common for the secondary bloom, which occurred in 33%–87% of the years depending on the region (Tables S1 and S2 in Supporting Information S1).

Although R3 presents relatively low Chl-a values, two blooms were identified, one in spring-summer (16th October–8th February) with mean b_k of 0.7 mg m^{-3}, and a secondary bloom in autumn-winter ($b_k = 0.63$ mg m^{-3}; 7th May–5th August). Also, R2 is characterized by two blooms with similar intensity, one in spring (b_k = 1.14 mg m^{-3}; 5th September–28th December) and one in autumn (b_k = 0.94 mg m^{-3}; 18th April–30th June). Frontal zones in R1 present a semi-annual cycle, with higher productivity in late spring-summer, with a bloom starting by the end of November (28th) and spanning for 107 days with a peak intensity of 1.36 mg m^{-3}.

The seasonal pattern of Patagonian temperate fronts in R5 agrees with the canonical cycles of temperate seas, where the chlorophyll maxima occur when the water column stratifies in early spring (26th September–5th Jane) with a secondary bloom that takes place during autumn (27th March–30th May). The peak value (b_k) for the spring bloom in R5 is one of the highest among all SOM regions (3.79 mg m^{-3}). Similarly, blooms in R4 start in early spring (b_i = 27th August) and span 91 days, reaching a b_k of 2.48 mg m^{-3}. During autumm, the peak is shorter and weaker, as revealed by b_d and b_k values (6th May–13th July, 2.1 mg m^{-3}).

In the Northwestern section of the shelf break (R7), the main bloom starts in early spring (b_i = 27th August) and ends in the beginning of summer (b_e = 7th Jan), with a mean peak intensity of 5.37 mg m^{-3}. With a lower probability of occurrence (33% of the calendar years), the second bloom starts in autumn (b_i = 12th April) and spans 75 days, with an intensity of 2.5 mg m^{-3}. In R8 and R6, corresponding to the location of the shelf-break, a single and extended spring-summer bloom (b_d = 173–177 days) starts by the end of September, with marked b_k differences (5.8 mg m^{-3} and 2.87 mg m^{-3}, respectively). The estuarine cold fronts of the Patagonian shelf (R9) have also an extended bloom in spring and summer (b_i = 15th October; b_e = 29th March; b_k = 3.01 mg m^{-3}).

Table 1
Trends of Sea Surface Temperature (SST, °C decade^{-1}), Mixed Layer Depth (MLD, m decade^{-1}), and Sea Surface Salinity (SSS, decade^{-1}) for Each Region Defined by Self-Organizing Maps Analysis (See Figure 2)

	SST		MLD		SSS	
	Trend	*p*	Trend	*p*	Trend	*p*
R1	**0.13 ± 0.02**	**<0.05**	−0.48	0.2	**−0.04 ± 0.004**	**<0.05**
R2	**0.26 ± 0.02**	**<0.05**	−0.43	0.28	−0.02	0.37
R3	**−0.06 ± 0.01**	**<0.05**	−0.35	0.71	−0.02	0.06
R4	0.09	0.07	**−1.52 ± 0.12**	**<0.05**	**−0.26 ± 0.01**	**<0.05**
R5	**0.08 ± 0.02**	**<0.05**	**−2.49 ± 0.17**	**<0.05**	**−0.19 ± 0.008**	**<0.05**
R6	**−0.15 ± 0.02**	**<0.05**	**1.8 ± 0.46**	**<0.05**	**−0.08 ± 0.008**	**<0.05**
R7	**0.08 ± 0.02**	**<0.05**	**−3.36 ± 0.13**	**<0.05**	**−0.18 ± 0.004**	**<0.05**
R8	**−0.09 ± 0.02**	**<0.05**	**−3.14 ± 0.19**	**<0.05**	**−0.12 ± 0.003**	**<0.05**
R9	−0.07	0.05	**−1.5 ± 0.23**	**<0.05**	**−0.15 ± 0.005**	**<0.05**

Note. Statistically significant trends are indicated in bold ($p < 0.05$).

3.3. Trends in Environmental Variables, Chl-a, and Phytoplankton Phenology

A positive significant trend of SST was observed in most of the biogeographical regions, with increases ranging between 0.07 ± 0.02 to 0.26 ± 0.03°C decade^{-1} (Table 1). Most dramatic changes (>0.2°C decade^{-1}) occur in R2, whereas trends in the rest of the regions average 0.07 ± 0.04°C decade^{-1}. Slight negative trends were observed in the rest of the regions, with more negative values in R8 and R6 (Malvinas Current; <−0.15 ± 0.03°C decade^{-1}, Table 1). Even though trends in MLD were more geographically variable, a significant negative trend was observed in most of the regions. The largest MLD reduction (<−2.4 ± 0.16 m decade^{-1}, Table 1) was restricted to regions R5, R7, and R8. Less productive regions (R1, R2, R3) did not present significant MLD trends. Likewise, SSS showed little to no significant trends in these regions. Conversely, salinity declines were observed over the highly productive shelf regions (−0.19 ± 0.04 decade^{-1}; R4, R5, R7, R9; Table 1).

As shown in Figure 4, except for R1, all regions display a significant positive trend in Chl-a, ranging between 0.03 ± 0.003 at R3 and 0.42 ± 0.04 mg m^{-3} decade^{-1} at R7. Regions in the shelf break area, in particular the northern transitional area (R7), showed the highest increases, where the peak intensity of the spring bloom showed a significant rise up to 1.4 ± 0.04 mg m^{-3} decade^{-1} (Figure 5). Also, the Patagonian temperate frontal region (R5) presents a significant Chl-a increase of 0.13 ± 0.001 mg m^{-3} decade^{-1}.

Significant trends for the main phenological indices are presented in Figure 5, for both main and the secondary blooms. The spring-summer bloom starts earlier in R1 (b_i = 28 ± 4 days decade^{-1}) and the bloom duration increases (b_d = 41 ± 11 days). Most changes were observed in the secondary blooms of regions R2, R3, R4, R5, R7. The number of autumn blooms in the 24 years analyzed was variable depending on the region considered, but in most regions, there was an increasing probability for a second bloom to occur (R2, R3, R4, R5, Table S2 in Supporting Information S1). Furthermore, three of the five regions presented at least one significant change in the phenology estimates (R2, R3, R5). R5 b_k increased 0.38 ± 0.08 mg m^{-3} decade^{-1}, and the start day was delayed (b_i = 24 ± 6 days decade^{-1}). Also, R2 registered a delay of the b_i, besides a delay of the bloom termination (b_e = 34 ± 4 days decade^{-1}; Figure 5). Finally, in R3 the autumn bloom increased slightly in peak intensity (0.09 ± 0.04 mg m^{-3} decade^{-1}), started earlier and end later, with the bloom duration lengthening by25 ± 5 days decade^{-1}.

4. Discussion

4.1. Biogeographical Regionalization and Phenological Characterization

An objective regionalization of the SWA has been proposed based on artificial neural networks applied to satellite Chl-a data. We have identified consistent biogeographical regions that correspond to different sub-basins characterized by distinct hydrodynamical, bathymetric, and/or ecological conditions. Two previous supervised and

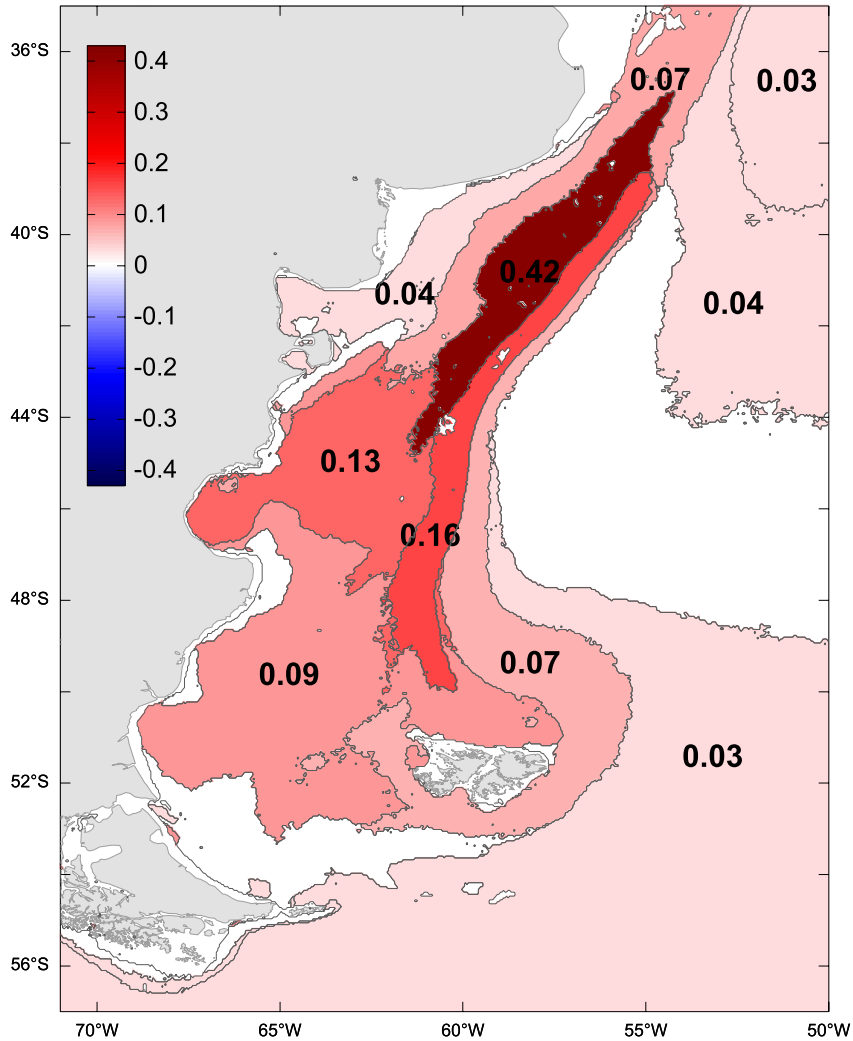

Figure 4. Statistically significant trends of Chl-a over the 24-year time series ($p < 0.05$) in the biogeographical regions of the SWA (mg m^{-3} $decade^{-1}$).

unsupervised regionalizations based on Chl-a, SST, and SST gradients have been performed for the north-eastern part of the study area (R1, R2, R3), but with only 6 years of data and lower spatial resolution (9 km) which resulted in 8 and 12 classes (Saraceno et al., 2005–2006, respectively). Our outcome in that area mostly coincides with the results presented by Saraceno et al. (2005–2006), where the R3, R2, and R1 are also separate regions located off the Patagonian Shelf.

The region extending over the largest area, R3, includes the oceanic waters off the Patagonian shelf, as well as the Burwood Bank, an undersea bank that represents a barrier to the northward flow of the Antarctic Circumpolar Current generating highly productive conditions that sustain important fisheries (Casarsa et al., 2019; García Alonso et al., 2018). Although it is recognized as a highly productive area, it presents relatively low Chl-a concentrations (Figure 1). According to Matano et al. (2019), potential explanations for these low Chl-a values would include insufficient light reaching the ocean surface, due to persistent cloud cover, deep mixing layers, and fast ocean currents. It has been also noticed that blooms, while still present, might not develop on the surface but subsurface waters, thus affecting satellite estimations (Guinder et al., 2020; Matano et al., 2019).

Two of the largest regions (R1 and R2), characterized by relatively low Chl-a concentrations, include areas of oceanic and coastal waters with the same temporal patterns of Chl-a variability, but with different mechanisms triggering blooms. R1 includes the tidal fronts of coastal Patagonia, which are defined by the boundary between the seasonally stratified mid-shelf column and the tidally mixed coastal waters. Stratification develops in the

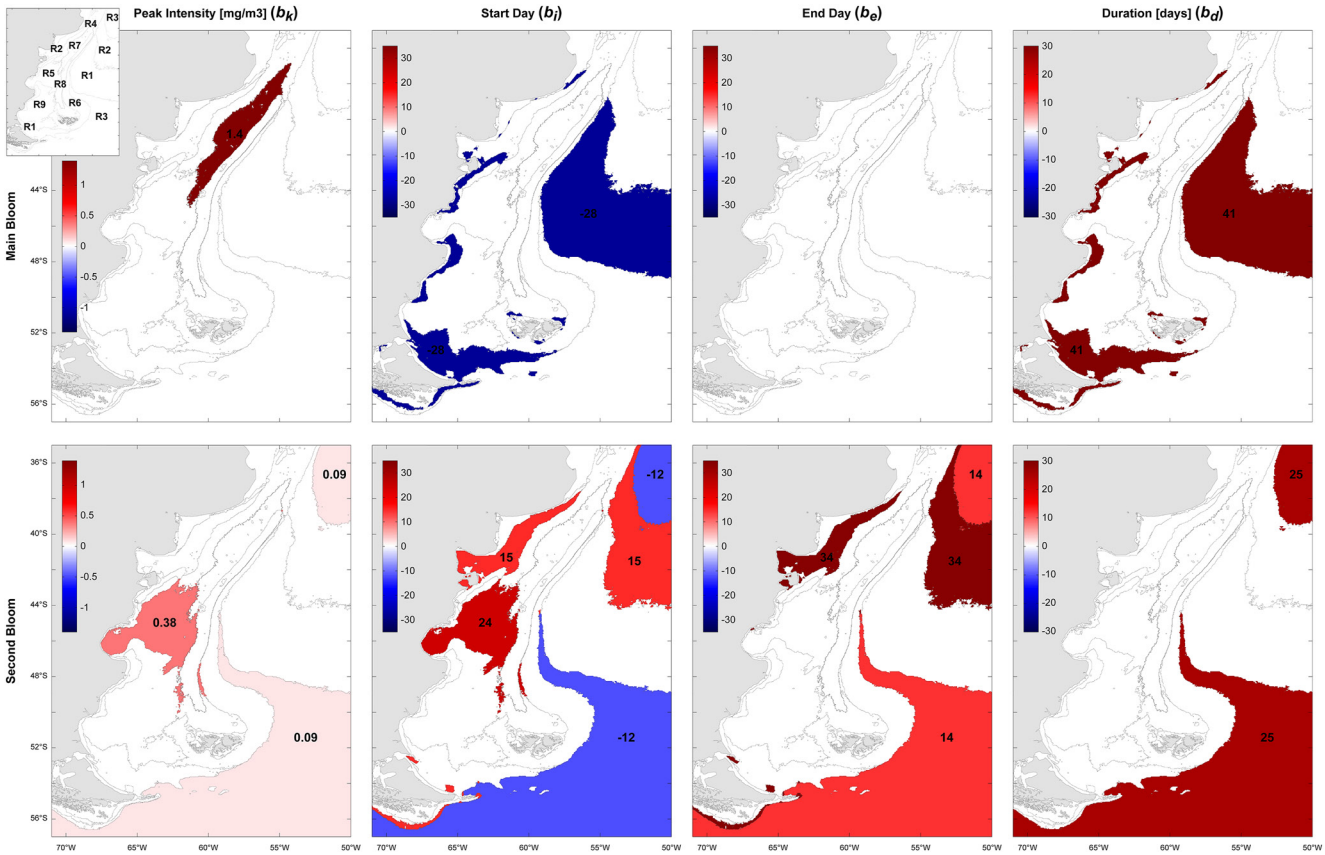

Figure 5. Trends of main and secondary phenological indices. b_k is presented in mg m^{-3} decade^{-1} and b_i, $b_{e,}$ and b_d in days decade^{-1}. Only the regions painted are statistically significant ($p < 0.05$).

mid-shelf during spring-summer allowing the occurrence of these biologically productive tidal fronts (Acha et al., 2004). R2, close to the coast, includes the Norpatagonian Gulfs and the area known as El Rincón (inner shelf). Previous studies in El Rincón area, based on in situ data, showed no clear seasonality in the Chl-a concentrations (Delgado et al., 2015). However, Williams et al. (2021) found a similar pattern to the one observed in our work for R2, in the inner section of the Gulf of San Matías. According to Williams et al. (2021) a first Chl-a peak occurs in spring, associated with the seasonal stratification of the water column, the bloom decays through summer as a result of nutrient limitation, and a second Chl-a maximum occurs in autumn, due to the nutrient replenishment that takes place as the mixing layer deepens. Off the Shelf, R1 and R2, encompass the retroreflection of the Brazil Current, and represents an eastward conduit of biogenic material (Signorini et al., 2009). The division in two different regions resulting from the SOM is in concordance with previous work by Saraceno et al. (2005) that described differences in Chl-a concentrations. Special attention should be given to the variability and trends of this area since is a source of productivity for the rest of the South Atlantic Ocean.

The physical mechanisms that trigger blooms in the mid-shelf (R5 and R4) are similar, but blooms exhibit phenological differences that result in different b_k, $b_{i,}$ and b_e. These differences are in agreement with the separation of two different regions by SOM. The Patagonian temperate fronts (R5) represent important spawning and nursery areas for several commercial species (e.g., Argentine red shrimp, Argentine hake, southern king crab; Segura et al., 2021). R4, in turn, is one of the main spring spawning and nursery areas for the northern population of *E. anochoita* (Marrari et al., 2013). Similar to R1 and R2, the seasonal patterns of R4 and R5 agree with the canonical cycle of temperate seas, where the Chl-a maxima are associated with the onset of stratification in spring, and the second smaller peak appears during automm when the thermocline weakens and deeper nutrient-rich waters entrain the surface layer (Akselman, 1996; Carreto et al., 1995; Rivas & Beier, 1990). In R5 both blooms start 1 month later than in R4, probably because of the later onset of stratification of the water column at this higher latitude. The strong Chl-a peak observed in R5 is consistent with previous observations in the San Jorge Gulf,

where bloom intensity reached ~9 mg m^{-3} in 2008 and high Chl-a values (>1.5 mg m^{-3}) persisted during summer (Figure 2 and Segura et al., 2021). The northern Patagonian mid-shelf front (R4) appears as a ~80 km band of high chlorophyll concentration offshore of the 50 m isobath. During spring-summer, the front develops, separating stratified waters (~>80 m offshore) from the vertically mixed nutrient-poor coastal waters of R2 (Lucas et al., 2005; Martos & Piccolo, 1988). The bloom ends at the beginning of summer due to the development of a strong thermal stratification and nutrient depletion in the euphotic layer (Carreto et al., 1995).

Within the shelf-break area, our bioregionalization allowed for the identification of three different regions, according to the different mechanisms triggering their blooms, and their sensitivity to environmental forces and changes. The northern region in the shelf-break area (R7) presents a high inter-annual variability, since it may present, depending on the environmental conditions of a given year, one single spring-summer bloom like the rest of the shelf-break (R8) or two blooms in spring and autumn, like the mid-shelf front (R4),. The complex structure of the shelf-break front in this area was analyzed by Franco et al. (2008), and a strong Chl-a gradient was described, perpendicular to the front, possibly caused by multiple branches of Malvinas Current. R6 is located between the 100 and 1,000 m isobaths, from 40°S to the northwestern border of Malvinas Islands and represents a transitional zone between the shelf-break front and the Atlantic Ocean. Although bloom initiation and duration are similar in R6 and R8, SOM classifies this area as a different region because the mean values of Chl-a and b_k, with magnitudes considerably lower (about a half) than the other two regions of the shelf-break.

Region R9, with a single annual bloom, encompasses the Patagonian cold estuarine zone, and extends from the outer region of the Peninsula Valdez front up to the northern area of the Malvinas Islands, overlapping with the southwestern portion of the shelf-break front. Water masses in this region are diluted due to low salinity waters coming from Southeast Pacific through the Le Marie Strait and the continental run-off of Patagonian main rivers (Dai & Trenberth, 2002; Lusquiños & Valdez, 1971). The diluted plume, mixed by strong tides and winds (westerlies) is traced to the 100 m isobath and south the San Jorge Gulf (Acha et al., 2004).

4.2. Trends in Environmental Variables, Chl-a, and Phytoplankton Phenology

Western boundary currents are expected to progressively warm as a result of the poleward migration of the subtropical ocean gyres. Indeed, the Brazil Current has been identified as one of the most extensive and intense surface warming hotspots globally (Hobday & Pecl, 2014). Our results (see R7 and R2 in Table 1) are consistent with recent studies reporting a warming trend of 0.4°C $decade^{-1}$ in the Brazil-Malvinas Confluence and the shelf-break front (e.g., Franco et al., 2020, 2022), as well as in the San Matías and Nuevo Gulfs (Williams & Nocera, 2023). Franco et al. (2022) suggested an intensification of the shelf-break front resulting from a cooling of the Malvinas Current (SST negative trend in R8, Table 1) and a warming of the adjacent shelf (SST positive trend in R7, Table 1). Also, the intensification of winds parallel to the front (Risaro et al., 2022) may enhance the turbulent mixing and increase the upwelling on the onshore side of the front (Franco et al., 2022). All these changes combined would benefit phytoplankton and increase their productivity.

Although the temporal stability of satellite products based on merging data from different sensors, such as Globcolour, should be carefully analyzed (Garnesson et al., 2019), in particular for trend computations, our results are consistent with previous positive phytoplankton biomass trends observed in the study area using two sensors (SeaWiFS and MODIS-Aqua: Marrari et al., 2017), or only one sensor (MODIS-Aqua: Franco et al., 2020; Williams & Nocera, 2023; SeaWiFS: Vantrepotte & Mélin, 2009). The significant trends in Chl-a concentration and phenology indices observed in this study may reflect changes in the functioning of the entire marine ecosystem, as they describe changes at the base of the food web. Several factors could be leading to Chl-a enhancement in the Argentine Shelf.

Consistently, our results indicate shallowing of the MLD in the Patagonian shelf (Table 1) as reported in previous studies (Franco et al., 2022; Williams & Nocera, 2023). According to Franco et al. (2022) the shallowing trend is stronger in the northwestern portion of the mid-shelf and the shelf-break, in agreement with the stronger trend observed in R7 of our study. Also, blooms in the shelf break front are typically diatom-dominated in early spring (MLD 40–80 m, nutrient-rich waters), and coccolithophores (*Emiliana huxeley*) dominate in summer when the MLD reaches its minimum (18 m) (Signorini et al., 2009). Thus, these smaller species could benefit from the shallowing of the MLD (~−3.3 m $decade^{-1}$) and the increasing trend in the Chl-a concentration may be due, not only to higher phytoplankton biomass but also to a change in dominance to coccolithophores, as their blooms

produce a high concentration of detached coccoliths (plates of calcium carbonate) characterized by a high reflectance (Holligan et al., 1993).

The most notable change observed in the present study is related to the timing of the secondary bloom. In R2 and R5, a delay in the start of the autumn bloom reaches 15 and 24 days, respectively. Secondary blooms occur in the austral autumn (Apr-May) when the thermocline weakens favoring the vertical supply of nutrient-rich waters to the euphotic zone (Akselman, 1996; Rivas & Beier, 1990). Thus, an extended warm period under a climate change scenario would delay the secondary bloom initialization.

5. Conclusions

The bioregionalization conducted in the present study allowed the identification, of 9 meaningful areas showing coherent patterns of Chl-a dynamics which are consistent with the oceanographic and biogeochemical characteristics of the Southwestern Atlantic Ocean. Regionalization facilitates and improves the analysis of environmental and biological changes in this extensive and highly complex region. The phenology of phytoplankton blooms in these coherent regions has been characterized, showing a main seasonal bloom in austral spring (September–December) and a secondary peak in austral autumn (March–June). Significant positive trends in total biomass have been registered in most regions, with higher Chl-a concentration increases in the shelf-break, especially in the northern area (R7). The remarkable increment in Chl-a concentration of R7 is attributed to frontal intensification caused by SST warming and MLD shoaling. In addition, changes in the frequency (more frequent), timing (earlier), and intensity (more intense) of the secondary (autumn) blooms are registered in regions corresponding to the Patagonian temperate front (R5) and the Norpatagonian Gulfs and El Rincón waters (R2). It is suggested that the significant warming trend of SST would sustain stratification for a longer period, thus delaying the secondary bloom initialization. Our results are expected to serve as a basis for future studies of the effects of climate change in this relevant ocean region.

Acknowledgments
The authors would like to thank the Consejo Nacional de Investigaciones Científicas y Técnicas (CONICET) for their financial support (BECA EXTERNA). This research was done in the frame of I-COOP 2021 project founded by the Consejo Superior de Investigaciones Científicas and the PICT2020-Serie A-02309 founded by the Agencia Nacional de Promoción de la Investigación, el Desarrollo Tecnológico y la Innovación. The present research was carried out within the framework of the activities of the Spanish Government through the "María de Maeztu Centre of Excellence" accreditation to IMEDEA (CSIC-UIB) (CEX2021-001198-M)." I. Hernandez-Carrasco acknowledges financial support from the project TRITOP (Grant: UIB2021-PD06) funded by University of the Balearic Islands and by FEDER(EU). V. Combes acknowledges the support of NSF Grants OCE-2149093, OCE-2149292, NASA award 80NSSC21K0559, and the support from the Spanish Ramón y Cajal Program (RYC2020-029306-I) through Grant AEI/UIB—10.13039/501100011033. J.S Font-Muñoz acknowledges funding by an individual postdoctoral fellowship "Margalida Comas" (PD/018/2020) from Govern de les Illes Balears and Fondo Social Europeo. P. Pratolongo thanks the financial support of Pampa Azul (B8). We all thank the GlobColour and Coopernicus groups for the distribution of satellite merged products and modeled data, respectively.

Data Availability Statement

For the SOM analysis, we used the SOM v.2.0 MATLAB toolbox (Vesanto et al., 2000) distributed by the Helsinki University of Technology (http://www.cis.hut.fi/somtoolbox/). The TIMESAT software was applied to obtain the phenological indices (Jönsson & Eklundh, 2004). The MATLAB Census X-13 toolbox was used to perform the Census X-13 analysis (Lengwiler, 2023) and the Sen's slope was estimated with the MATLAB Mann-Kendall Tau-b with Sen's Method (enhanced) (Burkey, 2023).

References

Acha, E. M., Mianzan, H. W., Guerrero, R. A., Favero, M., & Bava, J. (2004). Marine fronts at the continental shelves of austral South America: Physical and ecological processes. *Journal of Marine Systems*, *44*(1–2), 83–105. https://doi.org/10.1016/j.jmarsys.2003.09.005

Akselman, R. (1996). *Estudios ecológicos en el Golfo San Jorge y adyacencias (Atlántico Sudoccidental): Distribución, abundancia y variación estacional del fitoplancton en relación a factores Físico-químicos y la dinámica hidrológica*. Doctoral dissertation, Universidad de Buenos Aires. Facultad de Ciencias Exactas y Naturales. Retrieved from https://hdl.handle.net/20.500.12110/tesis_n2857_Akselman

Alvain, S., Moulin, C., Dandonneau, Y., & Loisel, H. (2008). Seasonal distribution and succession of dominant phytoplankton groups in the Global Ocean: A satellite view. *Global Biogeochemical Cycles*, *22*(3), GB3001. https://doi.org/10.1029/2007GB003154

Anderson, S. I., Barton, A. D., Clayton, S., Dutkiewicz, S., & Rynearson, T. A. (2021). Marine phytoplankton functional types exhibit diverse responses to thermal change. *Nature Communications*, *12*(1), 6413. https://doi.org/10.1038/s41467-021-26651-8

Armstrong, R. A., Gilbes, F., Guerrero, R., Lasta, C., Benavidez, H., & Mianzan, H. (2004). Validation of SeaWiFS-derived chlorophyll for the Rio de la Plata Estuary and adjacent waters. *International Journal of Remote Sensing*, *25*(7–8), 1501–1505. https://doi.org/10.1080/01431160310001592517

Artana, C., Provost, C., Lellouche, J. M., Rio, M. H., Ferrari, R., & Sennéchael, N. (2019). The Malvinas current at the confluence with the Brazil current: Inferences from 25 years of Mercator ocean reanalysis. *Journal of Geophysical Research: Oceans*, *124*(10), 7178–7200. https://doi.org/10.1029/2019JC015289

Basterretxea, G., Font-Muñoz, J. S., Salgado-Hernanz, P. M., Arrieta, J., & Hernández-Carrasco, I. (2018). Patterns of chlorophyll interannual variability in Mediterranean biogeographical regions. *Remote Sensing of Environment*, *215*, 7–17. https://doi.org/10.1016/j.rse.2018.05.027

Ben Mustapha, Z., Alvain, S., Jamet, C., Loisel, H., & Dessailly, D. (2014). Automatic classification of water-leaving radiance anomalies from global SeaWiFS imagery: Application to the detection of phytoplankton groups in open ocean waters. *Remote Sensing of Environment*, *146*, 97–112. https://doi.org/10.1016/j.rse.2013.08.046

Benzouaï, S., Louanchi, F., & Smara, Y. (2020). Phytoplankton phenology in Algerian continental shelf and slope waters using remotely sensed data. *Estuarine, Coastal and Shelf Science*, *247*, 107070. https://doi.org/10.1016/j.ecss.2020.107070

Burkey, J. (2023). Mann-Kendall Tau-b with Sen's method (enhanced). MATLAB Central File Exchange. Recuperado Retrieved from https://www.mathworks.com/matlabcentral/fileexchange/11190-mann-kendall-tau-b-with-sen-s-method-enhanced

Cai, W., McPhaden, M. J., Grimm, A. M., Rodrigues, R. R., Taschetto, A. S., Garreaud, R. D., et al. (2020). Climate impacts of the El Niño–southern oscillation on South America. *Nature Reviews Earth & Environment*, *1*(4), 215–231. https://doi.org/10.1038/s43017-020-0040-3

Carreto, J., Lutz, V. A., Carignan, M. O., Colleoni, A. D. C., & De Marco, S. G. (1995). Hydrography and chlorophyll a in a transect from the coast to the shelf-break in the Argentinian Sea. *Continental Shelf Research*, *15*(2–3), 315–336. https://doi.org/10.1016/0278-4343(94)E0001-3

Casarsa, L., Diez, M. J., Madirolas, A., Cabreira, A. G., & Buratti, C. C. (2019). Morphometric description of schools from two different stocks of the southernmost sprat Sprattus fuegensis. *Fisheries Research*, *212*, 29–34. https://doi.org/10.1016/j.fishres.2018.12.004

Dai, A., & Trenberth, K. (2002). Estimates of freshwater discharge from continents: Latitudinal and seasonal variations. *Journal of Hydrometeorology*, *3*(6), 660–667. https://doi.org/10.1175/1525-7541(2002)003<0660:eofdfc>2.0.co;2

Delgado, A. L., Guinder, V. A., Dogliotti, A. I., Zapperi, G., & Pratolongo, P. D. (2019). Validation of MODIS-Aqua bio-optical algorithms for phytoplankton absorption coefficient measurement in optically complex waters of El Rincón (Argentina). *Continental Shelf Research*, *173*, 73–86. https://doi.org/10.1016/j.csr.2018.12.012

Delgado, A. L., Loisel, H., Jamet, C., Vantrepotte, V., Perillo, G. M., & Piccolo, M. C. (2015). Seasonal and inter-annual analysis of chlorophyll-a and inherent optical properties from satellite observations in the inner and mid-shelves of the south of Buenos Aires Province (Argentina). *Remote Sensing*, *7*(9), 11821–11847. https://doi.org/10.3390/rs70911821

Delgado, A. L., Pratolongo, P. D., Dogliotti, A. I., Arena, M., Celleri, C., Cardona, J. E. G., & Martinez, A. (2021). Evaluation of MODIS-Aqua and OLCI Chlorophyll-a products in contrasting waters of the Southwestern Atlantic Ocean. *Ocean and Coastal Research*, *69*. https://doi.org/10.1590/2675-2824069.20-003ald

Dogliotti, A. I., Schloss, I. R., Almandoz, G. O., & Gagliardini, D. A. (2009). Evaluation of SeaWiFS and MODIS chlorophyll-a products in the Argentinean Patagonian continental shelf (38 S–55 S). *International Journal of Remote Sensing*, *30*(1), 251–273. https://doi.org/10.1080/01431160802311133

Doney, S. C., Ruckelshaus, M., Emmett Duffy, J., Barry, J. P., Chan, F., English, C. A., et al. (2012). Climate change impacts on marine ecosystems. *Annual Review of Marine Science*, *4*(1), 11–37. https://doi.org/10.1146/annurev-marine-041911-111611

Drévillon, M., Lellouche, J.-M., Réginer, C., Garric, G., Bricaud, C., Hernandez, O., & Bourdallé-Badie, R. (2022). Quality information document for global ocean reanalysis products. CMEMS-GLO-QUID-001-030.

Dutkiewicz, S., Scott, J. R., & Follows, M. J. (2013). Winners and losers: Ecological and biogeochemical changes in a warming ocean. *Global Biogeochemical Cycles*, *27*(2), 463–477. https://doi.org/10.1002/gbc.20042

Field, C. B., Behrenfeld, M. J., Randerson, J. T., & Falkowski, P. (1998). Primary production of the biosphere: Integrating terrestrial and oceanic components. *Science*, *281*(5374), 237–240. https://doi.org/10.1126/science.281.5374.237

Franco, B. C., Combes, V., & González Carman, V. (2020). Subsurface ocean warming hotspots and potential impacts on marine species: The southwest South Atlantic Ocean case study. *Frontiers in Marine Science*, *7*, 563394. https://doi.org/10.3389/fmars.2020.563394

Franco, B. C., Piola, A. R., Rivas, A. L., Baldoni, A., & Pisoni, J. P. (2008). Multiple thermal fronts near the Patagonian shelf break. *Geophysical Research Letters*, *35*(2), L02607. https://doi.org/10.1029/2007GL032066

Franco, B. C., Ruiz-Etcheverry, L. A., Marrari, M., Piola, A. R., & Matano, R. P. (2022). Climate change impacts on the Patagonian shelf break front. *Geophysical Research Letters*, *49*(4), e2021GL096513. https://doi.org/10.1029/2021GL096513

Friedlingstein, P., Jones, M. W., O'sullivan, M., Andrew, R. M., Hauck, J., Peters, G. P., et al. (2019). Global carbon budget 2019. *Earth System Science Data*, *11*(4), 1783–1838. https://doi.org/10.5194/essd-11-1783-2019

Garcia, V. M., Garcia, C. A., Mata, M. M., Pollery, R. C., Piola, A. R., Signorini, S. R., et al. (2008). Environmental factors controlling the phytoplankton blooms at the Patagonia shelf-break in spring. *Deep Sea Research Part I: Oceanographic Research Papers*, *55*(9), 1150–1166. https://doi.org/10.1016/j.dsr.2008.04.011

García Alonso, V. A., Brown, D., Martín, J., Pájaro, M., & Capitanio, F. L. (2018). Seasonal patterns of Patagonian sprat Sprattus fuegensis early life stages in an open sea Sub-Antarctic Marine Protected Area. *Polar Biology*, *41*(11), 2167–2179. https://doi.org/10.1007/s00300-018-2352-z

Garnesson, P., Mangin, A., Fanton d'Andon, O., Demaria, J., & Bretagnon, M. (2019). The CMEMS GlobColour chlorophyll a product based on satellite observation: Multi-sensor merging and flagging strategies. *Ocean Science*, *15*(3), 819–830. https://doi.org/10.5194/os-15-819-2019

Garzón-Cardona, J. E., Martínez, A., Pantoja, S., Guinder, V., Koch, B., Krock, B., et al. (2019). Linking optical and chemical signatures of dissolved organic matter in the southern Argentine shelf: Distribution and bioavailability. *Journal of Marine Systems*, *195*, 74–82. https://doi.org/10.1016/j.jmarsys.2019.03.010

Gilbert, R. O. (1987). *Statistical methods for environmental pollution monitoring*. John Wiley & Sons.

Guinder, V. A., Malits, A., Ferronato, C., Krock, B., Garzón-Cardona, J., & Martínez, A. (2020). Microbial plankton configuration in the epipelagic realm from the Beagle Channel to the Burdwood Bank, a marine Protected area in Sub-Antarctic waters. *PLoS One*, *15*(5), e0233156. https://doi.org/10.1371/journal.pone.0233156

Guinder, V. A., Tillmann, U., Krock, B., Delgado, A. L., Krohn, T., Garzón Cardona, J. E., et al. (2018). Plankton multiproxy analyses in the Northern Patagonian Shelf, Argentina: Community structure, phycotoxins, and characterization of toxic Alexandrium strains. *Frontiers in Marine Science*, *5*, 394. https://doi.org/10.3389/fmars.2018.00394

Henderson, R. (1916). Note on graduation by adjusted average. *Transactions of the Actuarial Society of America*, *17*, 43–48.

Hernández-Carrasco, I., & Orfila, A. (2018). The role of an intense front on the connectivity of the western Mediterranean Sea: The Cartagena-Tenes front. *Journal of Geophysical Research: Oceans*, *123*(6), 4398–4422. https://doi.org/10.1029/2017JC013613

Hirsch, R. M., Slack, J. R., & Smith, R. A. (1982). Techniques of trend analysis for monthly water quality data. *Water Resources Research*, *18*(1), 107–121. https://doi.org/10.1029/wr018i001p00107

Hobday, A. J., & Pecl, G. T. (2014). Identification of global marine hotspots: Sentinels for change and vanguards for adaptation action. *Reviews in Fish Biology and Fisheries*, *24*(2), 415–425. https://doi.org/10.1007/s11160-013-9326-6

Holligan, P. M., Fernández, E., Aiken, J., Balch, W. M., Boyd, P., Burkill, P. H., et al. (1993). A biogeochemical study of the coccolithophore, Emiliania huxleyi, in the North Atlantic. *Global Biogeochemical Cycles*, *7*(4), 879–900. https://doi.org/10.1029/93GB01731

Ibanez, F., & Conversi, A. (2002). Prediction of missing values and detection of "exceptional events" in a chronological planktonic series: A single algorithm. *Ecological Modelling*, *154*(1–2), 9–23. https://doi.org/10.1016/S0304-3800(02)00033-9

Jönsson, P., & Eklundh, L. (2004). TIMESAT—A program for analyzing time-series of satellite sensor data [Software]. Computers & Geosciences, *30*, 833–845. https://doi.org/10.1016/j.cageo.2004.05.006

Kohonen, T. (1982). Self-organized formation of topologically correct feature maps. *Biological Cybernetics*, *43*(1), 59–69. https://doi.org/10.1007/BF00337288

Kohonen, T. (1990). The self-organizing map. *Proceedings of the IEEE*, *78*(9), 1464–1480. https://doi.org/10.1109/5.58325

Lara, R. J., Alder, V., Franzosi, C. A., & Kattner, G. (2010). Characteristics of suspended particulate organic matter in the southwestern Atlantic: Influence of temperature, nutrient and phytoplankton features on the stable isotope signature. *Journal of Marine Systems*, *79*(1–2), 199–209. https://doi.org/10.1016/j.jmarsys.2009.09.002

Lellouche, J. M., Greiner, E., Le Galloudec, O., Garric, G., Regnier, C., Drevillon, M., et al. (2018). Recent updates to the Copernicus Marine Service global ocean monitoring and forecasting real-time 1/12∘ high-resolution system. *Ocean Science*, *14*(5), 1093–1126. https://doi.org/10.5194/os-14-1093-2018

Lengwiler, Y. (2023). X-13 toolbox for seasonal filtering MATLAB central file exchange [Software]. Mathworks. https://www.mathworks.com/matlabcentral/fileexchange/49120-x-13-toolbox-for-seasonal-filtering

Leyba, I. M., Solman, S. A., & Saraceno, M. (2019). Trends in sea surface temperature and air–sea heat fluxes over the South Atlantic Ocean. *Climate Dynamics*, *53*(7–8), 4141–4153. https://doi.org/10.1007/s00382-019-04777-2

Liu, Y., Weisberg, R. H., & Mooers, C. N. (2006). Performance evaluation of the self-organizing map for feature extraction. *Journal of Geophysical Research*, *111*(C5), C05018. https://doi.org/10.1029/2005JC003117

Liu, Y., Weisberg, R. H., Vignudelli, S., & Mitchum, G. T. (2016). Patterns of the loop current system and regions of sea surface height variability in the eastern Gulf of Mexico revealed by the self-organizing maps. *Journal of Geophysical Research: Oceans*, *121*(4), 2347–2366. *ical geography* of the sea. https://doi.org/10.1002/2015JC011493

Longhurst, A. R. (2007). Chapter 9—The Atlantic Ocean. In A. R. Longhurst (Ed.), *Ecological geography of the sea* (2nd ed., pp. 131–273). Academic Press.

Lucas, A. J., Guerrero, R. A., Mianzan, H. W., Acha, E. M., & Lasta, C. A. (2005). Coastal oceanographic regimes of the northern Argentine continental shelf (34–43 S). *Estuarine, Coastal and Shelf Science*, *65*(3), 405–420. https://doi.org/10.1016/j.ecss.2005.06.015

Lusquiños, A., & Valdez, A. (1971). *Aportes al conocimiento de las masas de agua del Atlántico Sudoccidental*. (Vol. 659, p. 42). Sericio de Hidrografía Naval.

Lutz, V. A., Segura, V., Dogliotti, A. I., Gagliardini, D. A., Bianchi, A. A., & Balestrini, C. F. (2010). Primary production in the Argentine Sea during spring estimated by field and satellite models. *Journal of Plankton Research*, *32*(2), 181–195. https://doi.org/10.1093/plankt/fbp117

Maritorena, S., d'Andon, O. H. F., Mangin, A., & Siegel, D. A. (2010). Merged satellite ocean color data products using a bio-optical model: Characteristics, benefits and issues. *Remote Sensing of Environment*, *114*(8), 1791–1804. https://doi.org/10.1016/j.rse.2010.04.002

Maritorena, S., & Siegel, D. A. (2005). Consistent merging of satellite ocean color data sets using a bio-optical model. *Remote Sensing of Environment*, *94*(4), 429–440. https://doi.org/10.1016/j.rse.2004.08.014

Marrari, M., Piola, A. R., & Valla, D. (2017). Variability and 20-year trends in satellite-derived surface chlorophyll concentrations in large marine ecosystems around south and western Central America. *Frontiers in Marine Science*, *4*, 372. https://doi.org/10.3389/fmars.2017.00372

Marrari, M., Signorini, S. R., McClain, C. R., Pájaro, M., Martos, P., Viñas, M. D., et al. (2013). Reproductive success of the Argentine anchovy, Engraulis anchoita, in relation to environmental variability at a mid-shelf front (Southwestern Atlantic Ocean). *Fisheries Oceanography*, *22*(3), 247–261. https://doi.org/10.1111/fog.12019

Martos, P., & Piccolo, M. C. (1988). Hydrography of the Argentine continental shelf between 38 and 42 S. *Continental Shelf Research*, *8*(9), 1043–1056. https://doi.org/10.1016/0278-4343(88)90038-6

Matano, R. P., Palma, E. D., & Combes, V. (2019). The Burdwood bank circulation. *Journal of Geophysical Research: Oceans*, *124*(10), 6904–6926. https://doi.org/10.1029/2019JC015001

Palmer, S. C., Odermatt, D., Hunter, P. D., Brockmann, C., Presing, M., Balzter, H., & Tóth, V. R. (2015). Satellite remote sensing of phytoplankton phenology in Lake Balaton using 10 years of MERIS observations. *Remote Sensing of Environment*, *158*, 441–452. https://doi.org/10.1016/j.rse.2014.11.021

Racault, M. F., Le Quéré, C., Buitenhuis, E., Sathyendranath, S., & Platt, T. (2012). Phytoplankton phenology in the global ocean. *Ecological Indicators*, *14*(1), 152–163. https://doi.org/10.1016/j.ecolind.2011.07.010

Risaro, D. B., Chidichimo, M. P., & Piola, A. R. (2022). Interannual variability and trends of sea surface temperature around Southern South America. *Frontiers in Marine Science*, *9*, 213. https://doi.org/10.3389/fmars.2022.829144

Rivas, A. L., & Beier, E. J. (1990). Temperature and salinity fields in the north patagonian gulfs. *Oceanologica Acta*, *13*(1), 15–20.

Salgado-Hernanz, P. M., Racault, M. F., Font-Muñoz, J. S., & Basterretxea, G. (2019). Trends in phytoplankton phenology in the Mediterranean Sea based on ocean-colour remote sensing. *Remote Sensing of Environment*, *221*, 50–64. https://doi.org/10.1016/j.rse.2018.10.036

Saraceno, M., Provost, C., & Lebbah, M. (2006). Biophysical regions identification using an artificial neuronal network: A case study in the South western Atlantic. *Advances in Space Research*, *37*(4), 793–805. https://doi.org/10.1016/j.asr.2005.11.005

Saraceno, M., Provost, C., & Piola, A. R. (2005). On the relationship between satellite-retrieved surface temperature fronts and chlorophyll a in the western South Atlantic. *Journal of Geophysical Research*, *110*(C11), C11016. https://doi.org/10.1029/2004JC002736

Sathyendranath, S., Brewin, R. J., Brockmann, C., Brotas, V., Calton, B., Chuprin, A., et al. (2019). An ocean-colour time series for use in climate studies: The experience of the ocean-colour climate change initiative (OC-CCI). *Sensors*, *19*(19), 4285. https://doi.org/10.3390/s19194285

Segura, V., Silva, R. I., Clara, M. L., Martos, P., Cozzolino, E., & Lutz, V. A. (2021). Primary production and plankton assemblages in the fisheries ground around San Jorge Gulf (Patagonia) during spring and summer. *Plankton and Benthos Research*, *16*(1), 24–39. https://doi.org/10.3800/pbr.16.24

Sen, P. K. (1968). Estimates of the regression coefficient based on Kendall's tau. *Journal of the American Statistical Association*, *63*(324), 1379–1389. https://doi.org/10.1080/01621459.1968.10480934

Shi, K., Zhang, Y., Zhang, Y., Li, N., Qin, B., Zhu, G., & Zhou, Y. (2019). Phenology of phytoplankton blooms in a trophic lake observed from long-term MODIS data. *Environmental Science & Technology*, *53*(5), 2324–2331. https://doi.org/10.1021/acs.est.8b06887

Shiskin, J. (1978). Seasonal adjustment of sensitive indicators. In *Seasonal analysis of economic time series* (pp. 97–104).

Sigman, D. M., Hain, M. P., & Haug, G. H. (2010). The polar ocean and glacial cycles in atmospheric CO_2 concentration. *Nature*, *466*(7302), 47–55. https://doi.org/10.1038/nature09149

Signorini, S. R., Garcia, V. M., Piola, A. R., Evangelista, H., McClain, C. R., Garcia, C. A., & Mata, M. M. (2009). Further studies on the physical and biogeochemical causes for large interannual changes in the Patagonian Shelf spring-summer phytoplankton bloom biomass (No. 200900836).

Spalding, M. D., Fox, H. E., Allen, G. R., Davidson, N., Ferdaña, Z. A., Finlayson, M. A. X., et al. (2007). Marine ecoregions of the world: A bioregionalization of coastal and shelf areas. *BioScience*, *57*(7), 573–583. https://doi.org/10.1641/B570707

Vantrepotte, V., & Mélin, F. (2009). Temporal variability of 10-year global SeaWiFS time-series of phytoplankton chlorophyll a concentration. *ICES Journal of Marine Science*, *66*(7), 1547–1556. https://doi.org/10.1093/icesjms/fsp107

Vantrepotte, V., & Mélin, F. (2011). Inter-annual variations in the SeaWiFS global chlorophyll a concentration (1997–2007). *Deep Sea Research Part I: Oceanographic Research Papers*, *58*(4), 429–441. https://doi.org/10.1016/j.dsr.2011.02.003

Vesanto, J., & Alhoniemi, E. (2000). Clustering of the self-organizing map. *IEEE Transactions on Neural Networks*, *11*(3), 586–600. https://doi.org/10.1109/72.846731

Vesanto, J., Himberg, J., Alhoniemi, E., Parhankangas, J., Team, S. O. M. T., & Oy, L. (2000). SOM toolbox for Matlab 5 [Software]. CIS, *57*. http://www.cis.hut.fi/somtoolbox/

Williams, G. N., Dogliotti, A. I., Zaidman, P., Solis, M., Narvarte, M. A., Gonzalez, R. C., et al. (2013). Assessment of remotely-sensed sea-surface temperature and chlorophyll-a concentration in San Matías Gulf (Patagonia, Argentina). *Continental Shelf Research*, *52*, 159–171. https://doi.org/10.1016/j.csr.2012.08.014

Williams, G. N., & Nocera, A. C. (2023). Bio-optical trends of waters around Valdés Biosphere Reserve: An assessment of the temporal variability based on 20 years of ocean color satellite data. *Marine Environmental Research*, *186*, 105923. https://doi.org/10.1016/j.marenvres.2023.105923

Williams, G. N., Pisoni, J. P., Solís, M. E., Romero, M. A., Ocampo-Reinaldo, M., Svendsen, G. M., et al. (2021). Variability of phytoplankton biomass and environmental drivers in a semi-enclosed coastal ecosystem (San Matías Gulf, Patagonian Continental Shelf, Argentina) using ocean color remote sensing (MODIS) and oceanographic field data: Implications for fishery resources. *Journal of Marine Systems*, *224*, 103615. https://doi.org/10.1016/j.jmarsys.2021.103615

Yala, K., Niang, N. D., Brajard, J., Mejia, C., Ouattara, M., El Hourany, R., et al. (2020). Estimation of phytoplankton pigments from ocean-color satellite observations in the Senegalo–Mauritanian region by using an advanced neural classifier. *Ocean Science*, *16*(2), 513–533. https://doi.org/10.5194/os-16-513-2020

Yu, S., Bai, Y., He, X., Li, T., & Gong, F. (2023). A new merged dataset of global ocean chlorophyll-a concentration for better trend detection. *Frontiers in Marine Science*, *10*, 48. https://doi.org/10.3389/fmars.2023.1051619

Zhai, L., Platt, T., Tang, C., Sathyendranath, S., & Walne, A. (2013). The response of phytoplankton to climate variability associated with the North Atlantic Oscillation. *Deep Sea Research Part II: Topical Studies in Oceanography*, *93*, 159–168. https://doi.org/10.1016/j.dsr2.2013.04.009

Zoljoodi, M., Moradi, M., & Moradi, N. (2022). Seasonal and interannual cycles of total phytoplankton phenology metrics in the Persian Gulf using ocean color remote sensing. *Continental Shelf Research*, *237*, 104685. https://doi.org/10.1016/j.csr.2022.104685